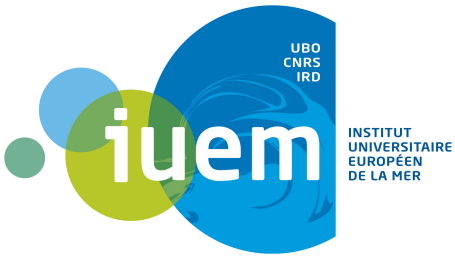

Front dynamics, between the inflowing Indian Ocean Surface Water, and the outflowing Persian Gulf water, from the observations of 2014

Author:
Coppin. M
Master 1 Marine Physics

Supervisor:
Pr. Xavier Carton
Dr. Pierre L'Hégaret

Référent:
Pr. Steven Herbette

May/June 2022

Contents

Abstract

In the Persian Gulf, inflowing Indian Ocean surface water meets the warmer, saltier water formed inside the Gulf and generates a haline front. The dynamics of these fronts and the effect of mesoscale structure on salinity distribution have been studied. A dynamic diagnosis and a survey on the vertical structure of the water column were made with data from the PHYSINDIEN2 2014 campaign, the GECKO observation product and the CMEMS reanalysis. The study period was divided into two parts of 4 days. In the first part, two counter-rotating vortex dipoles were identified, as well as two dipoles of the same nature and a vortex tripole with the same direction of rotation in the second part. The frontogenesis study allowed to diagnose the surface behaviours of the fronts and their evolution over the two periods. A diagnosis of the vertical distribution of salinity and frontogenesis allowed a more detailed description of the fronts and their dynamics. This showed that the front separates the more homogenous zones from the more stratified ones. Finally the difficulty to describe the dynamics only with the altimetric tools is given.

Key words: Persian Gulf, fronts dynamics, Frontogenesis, Mesoscale eddy, salinity distribustion,

1 Introduction

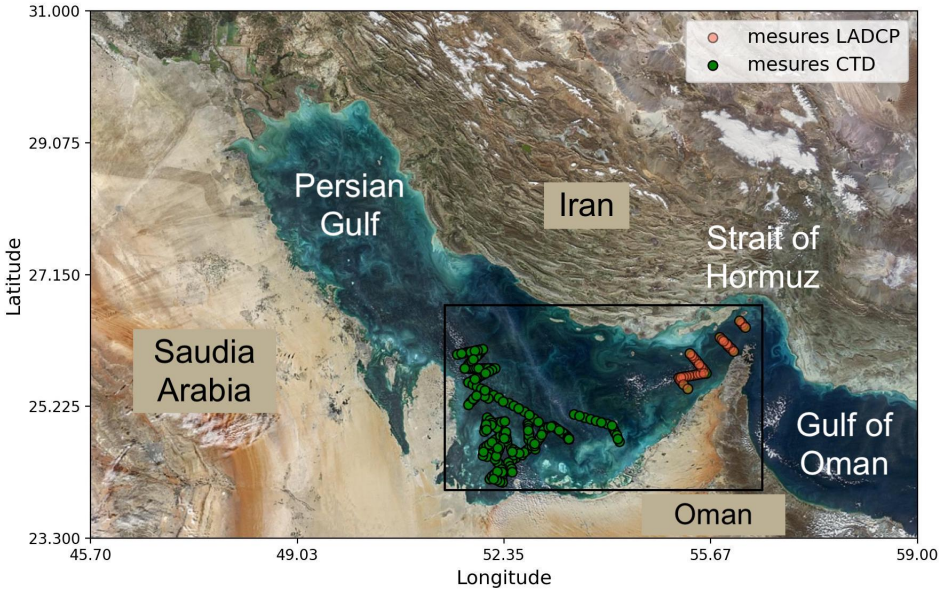

Figure 1: Chart of the Arabian/Persian Gulf, Strait of Hormuz and Gulf of Oman and the CTD and LADCP profil of the PHISINDIEN 2014 campagne

The Persian Gulf (herafter call the Gulf) is a semi-enclosed basin surrounded, to the west, by flat land, but by mountains at the North-East. The average depth is about 40 m but reaches a maximum of 120 m near the Strait of Hormuz wich connects the Gulf to the Gulf of Oman. It is a Northwest to Southeast oriented basin with lengh of about 1000 km and a maximum width of 350km

for a surface of about 239,000km^2. Its climates contains an high intra-annual variability impacted by the monsoon oscillation, that drive with winds the basin-scale circulation. The mean circulation is composed by a cyclonic gyre growing from April to July in the southern basin. It is accompanied by an anticylonic gyre in the northwest basin between June and August. Then as the year progresses the cyclonic gyre tends to shrink, and break into smaller eddies (Pous. et al, 2012). The Gulf has a very weak precipitation rate of about 15 $cm/year$ whearas the evaporation is strong with a value often estimated at 200 $cm/year$. The discharge of the Tigrus, Euphrates and Karun river which form the Shatt-al-arab have an annual mean of 1400 m^3. The discharges of the Iranian rivers, less known, are estimated to 2000m^3 .That leads to a net 416$km^3/year$ water deficit compensated by the inflow of a fresher and less saline water from the Oman sea through the Strait of Hormuz. This inflow is composed of IOSW (Indian Ocean Surface water).

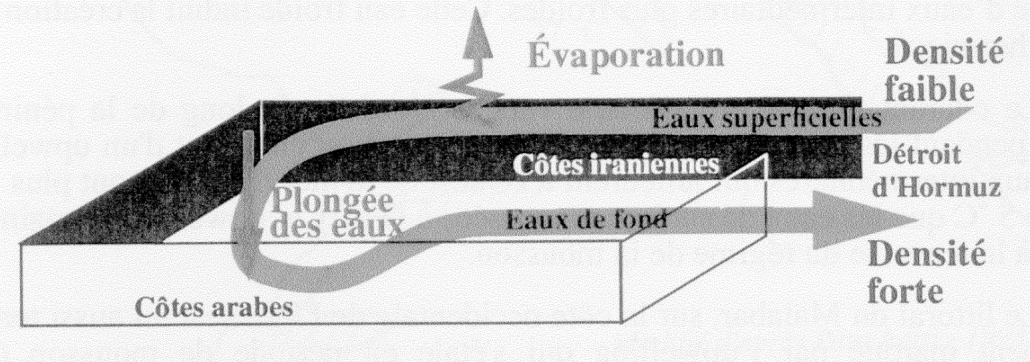

Figure 2: Schematic illustration of the Persian Gulf circulation. From *FSOR : Golfe Persique - Golfe d'Oman, 1998.*

The region we are interested in, is more precisely the south of the Gulf. Motivations for studying this region are that the Gulf is very shallow, subject to strong forcing and is of high complexity. Thus, the theoretical knowledge and the lack of in situ observations do not allow a modelization as accurate as in the rest of the ocean. Furthermore it is a basin that forms very particular waters whose salinity can reach 50 psu and whose signatures can be fond in the Indian Ocean. But also because it is an evaporation basin in which we suspect that the impact of climate change is and will be important.

Earlier studies evaluated the dynamical characteristics and variability of those salty water fronts (Bidokhti et al., 2018) using the HYCOM numerical model compared to ROPME project's observations in 1992 (Reynolds., 1993) near the strait..

We propose here to give an analysis of in situ data obtained during the PHYSINDIEN campaign in 2014 led by the SHOM and satellite data, with the CMEMS product, to investigate the dynamics of the haline front and the general dynamics of the region, the meso-structures and their effects on the stratification in the southern part of the Gulf.

This study is the continuation of a previous internship which aimed to analyze the tidal signal in the southern Gulf.

This report is presented as follows :

- The data sets used end the method used are described hereafter
- A first general description of the salinity distribution and the dynamics of the Gulf at the surface
- Then a more detailed diagnostics of the different components of the velocity field that act on the water masses

- A description of the main dynamical structures.
- An identification of the water masses present and a comparative study of the salinity sections with their dynamic profiles
- A discussion about the various results obtained, and their validity with some perspectives

2 Materials and Methods

2.1 Materials

As mentioned above, the novelty of this study is the cross use of in situ data, satellite data and model data, with a new in situ dataset.

2.1.1 In situ observation

The in situ data were collected during the PHYSINDIEN2 2014 campaign managed by the SHOM (Service Hydrographique et Oceanographique de la Marine). This campaign is a continuation of the previous PHYSINDIEN campaigns conducted in spring 2011 and 2014. These campaigns aim to study the hydrology and dynamics of water columns around the Arabian Peninsula, from the Red Sea to the Persian Gulf. The ship, Beautemps-Beaupré, has deployed a CTD (Conductivity Themperature density) , SIPPICAN, LADCP and ADCP (Acoustic Doppler Current Profiler). The temperature and salinity data have an accuracy of 10^{-3} °C and 10^{-3} psu. This study will focus only on salinity and temperature data in the southernof the Gulf relaying on 340 vertical profiles divided into 28 sections. The data sets provide values of practical salinity and in situ temperature. These variables are converted into absolute salinity and conservative temperature using the Gibbs SeaWater (GSW) Oceanographic Toolbox of TEOS-10 (https://www.teos-10.org/)(McDougall and Barker, 2011).

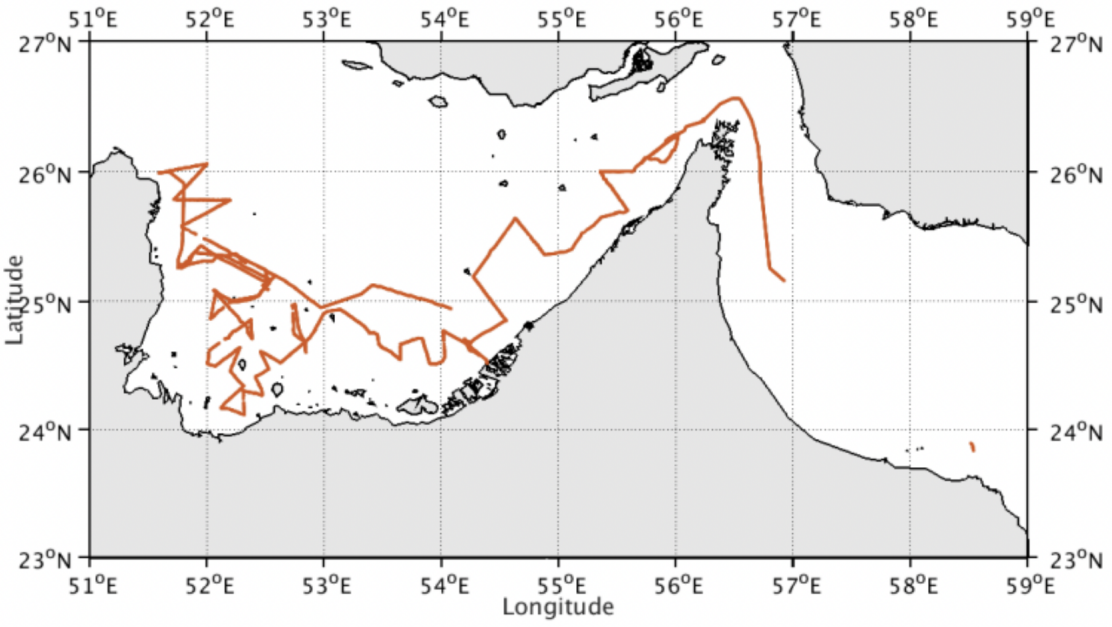

Figure 3: Trajectory of the oceanographic ship Beautemps-Beaupré during the PHYSINDIEN 2014 campaign

2.1.2 Satellite data

Satellite data have been used to give an overall view, at low spatial resolution but with a useful sufficient repetitivity to evaluate the evolution of mesoscale structures and a diagnosis of the surface dynamics. The tool used is the GECKO product available on (www.legos.obs-mip.fr/sudre/mesoscale-oceanic-current-extracting-program). Its principle is to combine the geostrophic component of the velocity field with the Ekman component (J. Sudre et al., 2013) The geostrophic components are computed from Aviso satellite altimetry data (Archiving, Validation and Interpretation of Satellite Oceanographic data) (www.aviso.oceanobs.com/en/data/productsinformation/ duacs)

$$u_g = -\frac{g}{f}\partial_y h$$

$$v_g = \frac{g}{f}\partial_x h$$

with u_g, v_g the geostrophic velocity, f the coriolis parameter, h the sea surface elevation.
The wind speed field components are evaluated from the mean wind field data from the ku-band microwave scatterometer (SeaWinds) onboard the QuikSCAT satellite, distributed by the Centre ERS d'Archivage et de Traitement (CERSAT). The data set obtained provides the wind stress in x and y coordinate, the ekman, geostrophic and total velocity field and the SLA (sea level anomaly). The spatial resolution of the product is 1/4°.

2.1.3 Model

The dynamics of the Gulf was studied using the GLORYS12V1 product which is based on the NEMO model with the real-time global forecasting CMEMS (https://doi.org/10.48670/moi-00021) as input. Hereafter it is called the CMEMS product. The product is a reanalysis that tends toward the altimetric observations at the surface. The data sets obtained are 3D on 50 vertical levels with a horizontal accuracy of 1/12° (approximately 8 km). The data used are potential temperature, practical salinity and, the velocity field from which the whole dynamical analysis is based.

The NEMO (for Nucleus for European Modelling of the Ocean) model (https://doi.org/10.5281/zenodo.633465 has as main hypotheses the spherical Earth approximation, the Thin-shell approximation, Boussinesq and Incompressibility hypotheses and it neglects the additional Coriolis terms. It has the primitive set of equations.
The momentum balance

$$\frac{\partial U_h}{\partial t} = -[(\nabla \times U) \times U + \frac{1}{2}\nabla(U^2)]_h - f.k \times U_h - \frac{1}{\rho_0}\nabla_h p + D^U + F^U$$

The heat and salt conservation equations

$$\frac{\partial T}{\partial t} = -\nabla.(TU) + D^T + F^T$$

$$\frac{\partial S}{\partial t} = -\nabla.(SU) + D^S + F^S$$

with U_h the horizontal componante of the velocity, D^J the parametrisation of small-scall physics and F^J the surface forcing terms. $J = U, S, T$

2.1.4 Synopticity of comparaison

Since we are studying a large area in a closed basin and not along track, satellite data have a spatial resolution that is the result of an interpolation and therefore subject to local errors. But it provides the best temporal sampling. The in situ data reveal the real situation along the sections with a high accuracy but a relatively small extent and only at a given time. They are subject to aliasing which is problematic in this region where mesoscale and sub-mesoscale structures evolve very rapidly. - The models are the datasets that allow the most dynamic study of the structure and fronts at fine scales because they have complete data on the entire water column with a fairly fine precision. However, their coherence is sometimes questioned, especially far from the satellite tracks from which their reanalysis is made.

2.2 Methodes

The data are gathered over intervals of 4 days in order to cut the PHYSINDIEN campaign in twohalves. The study of the salt distribution and the dynamics in the basin are divided into two parts.

The first part consists in a surface diagnostic of the salinity distribution with its front. To determine the general dynamics of the area and the main structures, the first step is to describe the surface salinity obtained from the CMEMS product by plotting the isohalines.Thus we get a first sketch of the salinity distribution in the Gulf of its gradient. Then the effect of surface currents on the salinity gradient is investigated by means of the frontogenesis function (Hoskins, 1982; McWilliams, 2021; Cassianides et al., 2020). This function at the surface determines the region of convergence and divergence of the salinity. Depending on the sign, it gives information on the increase or relaxation of the gradient salinity and therefore on the formation of a front. We assume that the evaporation minus precipitation, and the diffusion $\nu\nabla^2 S$ are weak as detailed in appendix.
Thus $\frac{dS}{dt} = 0$. Considering the salinity conserved is a good assumption for the time scale we are intereted in (4 days).
Frontogenesis function :

$$\frac{1}{2}\partial_t \ \|\nabla \mathbf{S}\|^{\mathbf{2}} = -\nabla \mathbf{S}\nabla \mathbf{u}.\nabla \mathbf{S} = \mathbf{F}$$

with S the salinity and u the velocity.

Then the determination of the weight of each component of the motion is determined by using the output of the Gecko and CMEMS products and determine the contribution of the Ekman and geostrophic currents. The tidal component is based on the study of S. Pous, X. Carton, P. Lazure (2012)

Finally the detection of the mesoscale eddies at the surface is performed from the CMEMS horizontal velocity data (U, V) by computing the Okubo-Weiss parameter (Okubo, 1970; Weiss 1991) :

$$OW = \sigma_{strain}^2 + \sigma_{shear}^2 - \omega^2$$

with :

the shear : $\sigma_{shear} = \partial_x V + \partial_y U$

the strain : $\sigma_{strain} = \partial_x U - \partial_y V$

the relative vorticity : $\omega = \partial_x V - \partial_y U$

This parameter is a good indicator of coherentestructures, positive (resp. negative) value indicate the region where the rotation (resp. deformation) dominate.

A more detailed diagnostic is made using the Okubo-Weiss parameter and the relative vorticity, in order to define the orientation of the vortices.

The second part is devoted to the study of the vertical salinity structure and front dynamics. For this purpose, the measurement profiles obtained from the PHSINDIEN2 2014 campaign are collected in sections, linearly interpolated on the vertical with a step $dz = 5cm$. The sectionsare oriented by convention from west to east. The sections of salinity are plotted with the matplotlib contourf function which itself performs a horizontal interpolation. The CMEMS product grid points are searched by the nearest neighbour method in order to create a section closest to that done by the Beautemps-Beaupré. The same method was then applied to the salinity and dynamics data from which the vorticity, Okubo-Weiss parameter and frontongenesis function were calculated.

Then we look at the stratification with the Simpson-Hunter criterion, obtained in the region from the HYCOM model computed by Pitek (2022). This criterion distinguishes the homogeneous regions from stratified ones by calculating the tidal energy necessary to mix the water column. it compares h/u_t^3 to 6.2 an observed critical value. If the result is inferior, the water column is more likely mixed by the tide. With h the water depth and u_t the tidal energy.

3 Results

3.1 *Dynamics of the region*

3.1.1 Salinity structure

Figure 4 a), b) show the salinity distribution at the surface for two time frames of the PHYSINDIEN campaign, between the 21 and the 25 May 2014, then between the 26 and the 30 May 2014. The salty water is concentrated in the south of the Gulf as shown by previous studies (Reynolds., 1993; Pous et al,. 2014, Pitek,. 2022) with a maximum of 39.7 psu.

The isohaline follows the coast in the south-east of the bassin with a regular gradient. At the south-west of the basin the haline gradient become perpendicular to the coast and stronger moving along the coast of Qatar. The intrusion of fresher water at the tip of Qatar is likely to come from the plume of the Shatt-al-arab, is consistent with the results obtained for a northwesterly wind like the Shamal (Pous,. phd 2005)

The salty water is trapped between the plume water coming from the north of the Gulf ,and the Oman gulf water inflowing through the Strait of Hormuz and flowing along the coast of Iran. This salinity structure remains the same for the two periods of the campaign.

At 53° East, water entering through the Hormuz Strait is drawn southwards by a cyclonic gyre which is present in spring and summer (Pous et al., 2014). Thus, cooler water is advected southwards while saltier water from the south of the basin is advected northwards. This explains the incursion of saltier water to the northeast of the region. Furthermore, the movement of this gyre can be also deduced by looking at the evolution of this incursion between period 1 and period 2 of the campaign.

3.1.2 Haline Frontogenesis

Though a front is difficult to define rigorously, one definition is given by Hoskins (Hoskins., 1982). He considers a front as " a region whose lengh scale is comparable with the radius of deformation in one direction but much smaller than this in the cross direction, and across which there are significant changes in buoyancy and velocity with gradient tending to become very large in a finite time. ". We define a salinity front in a more quantitative way based on isohaline observations. Isohaline narrowing

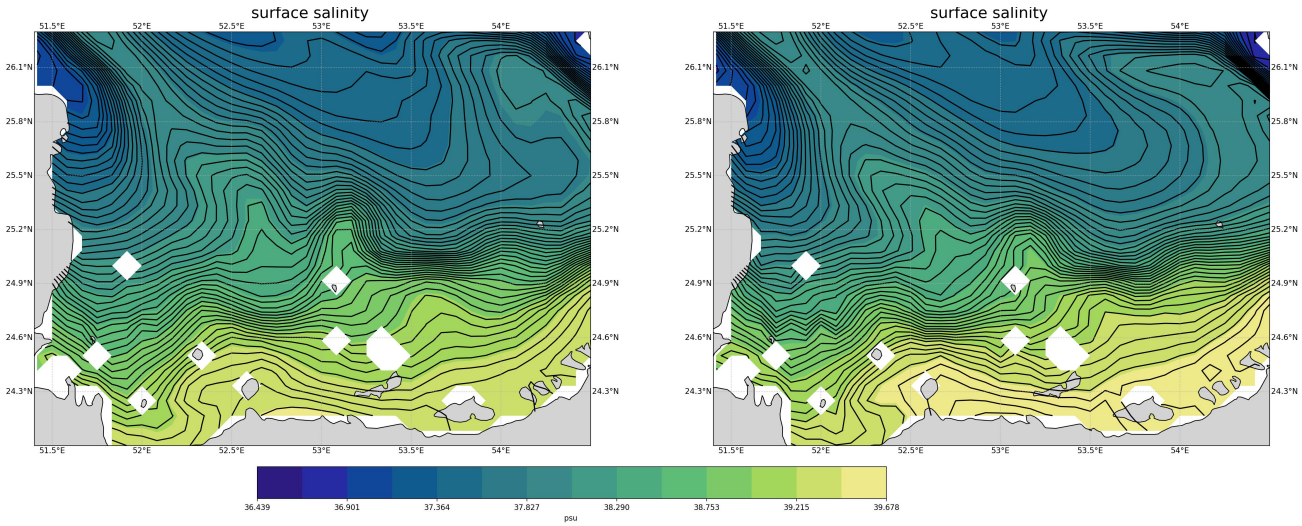

Figure 4: Sea Surface salinity with isohalines computed from CMEMS. Left panel: the first period of the campaign (21-25 May 2014), right panel: the second period (26-30 May 2014)

is found adjacent to the inflow of fresh water from the north, in the area at 24.6°N between 52.5°E and 52.7°E, and also in the area at 24.9°N between 53.3°E and 55°E. Also noticeable in the northeast is an area with a very strong salinity gradient which represents the front between the incoming water from the Hormuz Strait and the water from the Persian Gulf.

On Figure 5, the surface salinity frontogenesis function is computed, revealing in red (resp. blue) the region of accentuation (resp. relaxation) of the salinity gradient. The result is consistant with the preliminary localisation of the front using the isohaline. Indeed the region with the strongest front between 24.9°N -25.5°and 53°E - 54°E and between 24.6°N -24.8°and 52.5°E - 53°E. An important result is that the salinity frontogenes is coherent and evolves in the time frame of 4 days. The intensification of the salinity gradient is more important in the second part of the campaign. Bellow we will see that this is due to the strengthening of the Ekman velocity which significantly intensifies the mesoscale structures and currents in the shallow areas.

3.1.3 *Dynamical component*

The Persian gGulf has a tidal oscillation period between 21.6 and 27 hours (Defant 1961). In March 2014, measurments indicated periods between 18 and 27 hours depending on the position and on the tidal component (Pitek, 2022). This period is kept in mind for the interpretation of the results especially for the long section because the front moves with the tidal wave. Furthermore semi-diurnal and diurnal waves interact into the basin due to it particular geometry leading to a system of amphidromic points of Kelvin-Taylor type (Pous et al., 2012). One of this amphidromic points is situated at the very center of the region we study. The maximum velocities due to tidal currents are estimated between 0.4 and 0.6 $m.s^{-1}$ even though the residual current, forming an anticyclonic current along the coast of Qatar, remains weak, of the order of $2cm.s^{-1}$ (Pous et al., 2012)

Geostrophic currents and wind stress induced velocities are the other components of the velocity field in the Gulf. Figure 6 shows the part of the geostrophic component in the velocity field for the Gecko product and for the CMEMS product. Gecko seems to be mainly driven by the geostrophic component in the whole basin whereas this component is less important in the southern part of the basin for the CMEMS product. The latter result seems more coherent because in this region of the

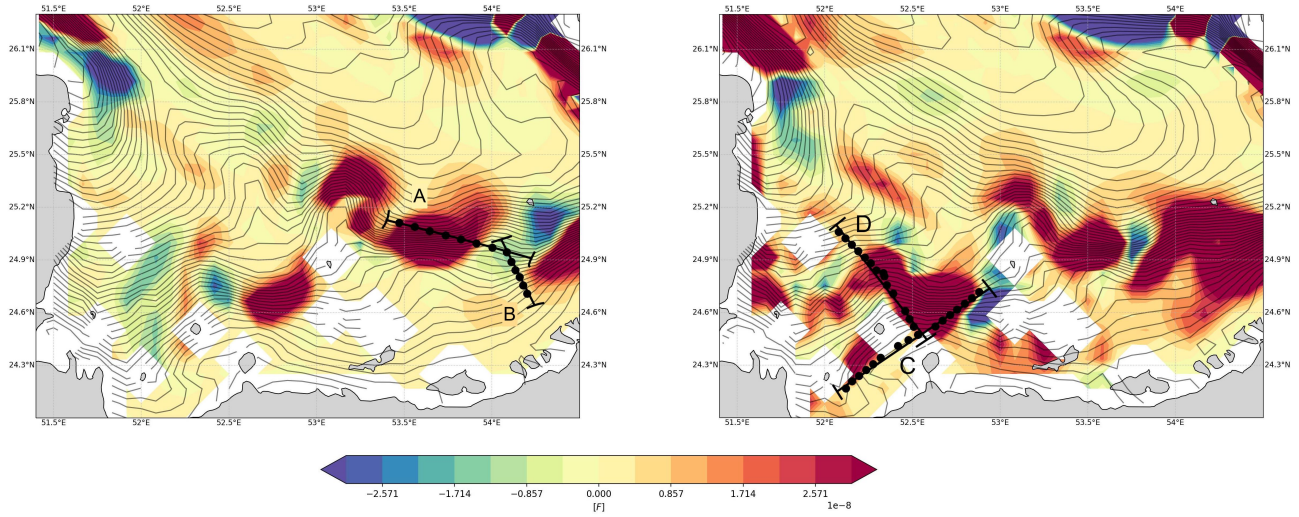

Figure 5: Salinity frontogenesis with isohaline computed from CMEMS. Left panel: the first period of the campaign (21-25 May 2014), right panel: the second period (26-30 May 2014)

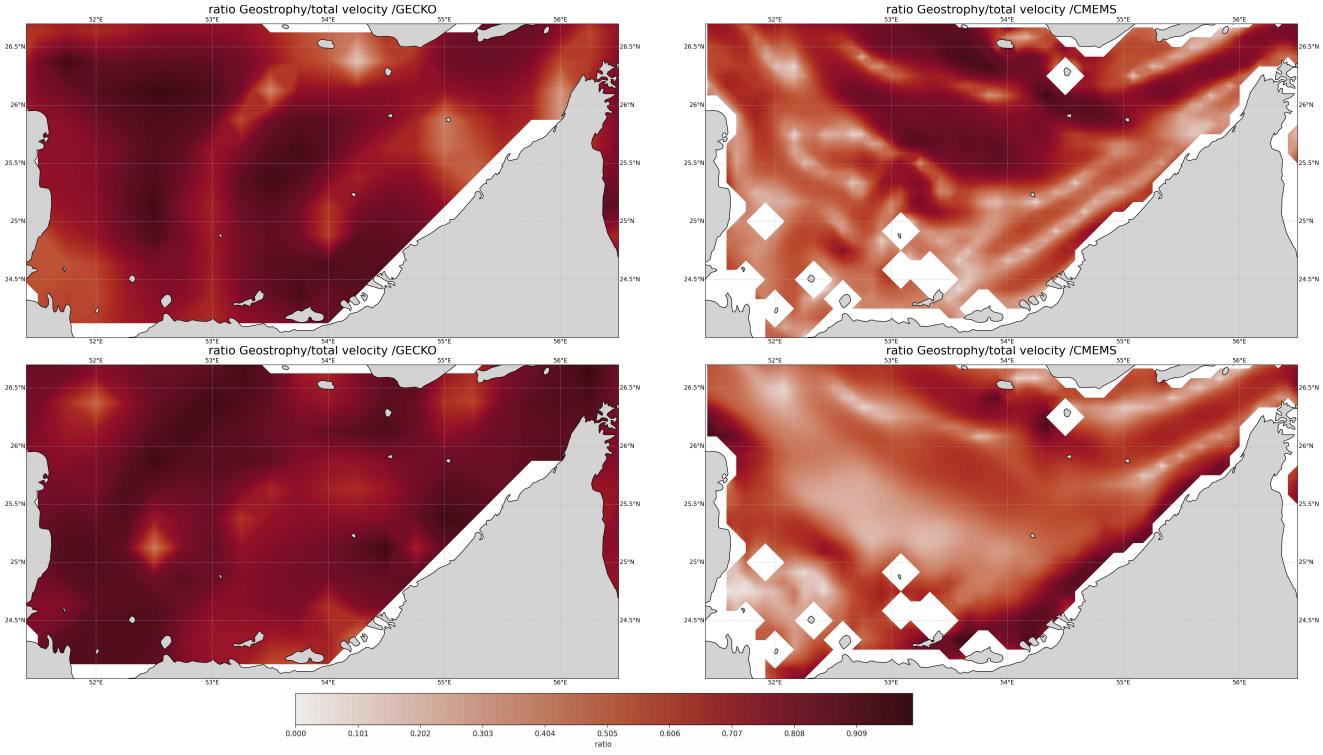

Figure 6: Ratio of the geostrophic velocity over the other components of the velocity for the GECKO data (left); the CMEMS model (right) for the two periods 21-25 May 2014 (top); 26-30 May 2014 (lower)

Gulf the depth varies from 10 to 20 m so the Ekman layer occupies the whole water column. The geostrophic component of the velocity naturally dominates less in these shallow regions. Figure 7 shows the Ekman component of the surface velocity over the two survey periods. The northwesterly Shamal wind is clearly visible.

Thus the dynamics in the southern Gulf is mainly impacted by the tide with an amphidromic point located in the center of the southern basin and by the Ekman currents whose direction remains relatively aligned on the shamal which is the axis of the basin (Northwest, South-East), the depth being too small to give rise to an Ekman spiral.

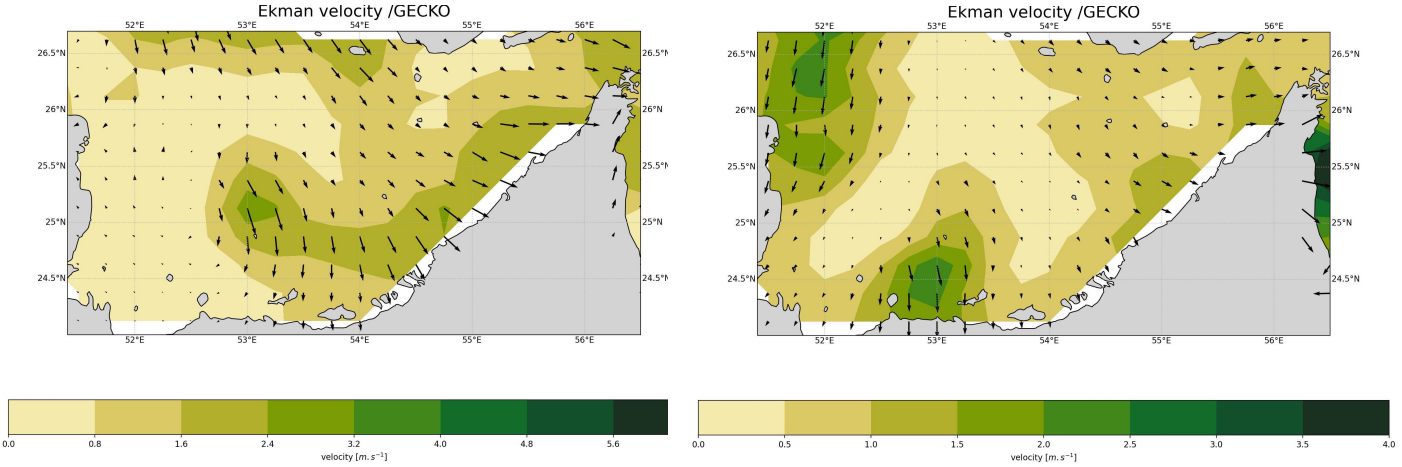

Figure 7: Ekman velocity componate for the two periode 21-25 may 2014 (left); 26-30 may 2014 (right)

3.2 *Main meso-structures*

A first structure has been identified, it is the cyclonic gyre located to the north-east of the region we are studying, along the Iranian coast,. This gyre is resident from April to July (Pous et al., 2015) and can be considered as synoptic in our study time. Smaller structures, mesoscale eddies, are identified in Figure 8. The Okubo Weiss parameter indicates the regions where rotation dominates deformation (in blue). Thus a first result is that the second period studied has many more structures in the southern region while they are less intense in the northern region. This tells us about the longevity of the mesoscales eddies in this region, which as we can see evolve on a time scale of about 4 days. In the first period, the isohalines are bent at the location of these meso structures in the direction of their rotation. The gradient is maximal at the centre of each dipole. In the second period, a quadrupole composed of two counter-rotating dipoles (3,4) and a tripole with vortices of the same direction of rotation (5,6) can be identified. The effects observed at the centre of a dipole with a vortex of opposite rotational direction are the same as for period 1, the isohalines are tightened and advected in the direction of rotation of the vortex. However, we observe that at the centre of dipole 5 with the same direction of rotation, the salinity gradient is relaxed. Nothing can be deduced from dipole 6.

Thus the haline front is deformed and curved in the (Oxy) plane according to the direction of rotation of the vortices. It is reinforced at the centre of a dipole of a counter-rotating vortex but appears relaxed between two vortices of the same direction.

3.3 *Stratification in the South of the basin through the salinity front*

3.3.1 Hydrological features

The water near the Hormuz Strait is divided into two masses, the PGW (Persian Gulf Water) coming out of the Gulf, and the IOSW. Both of them are present in the same water column, resulting in mixing, which explains the trend in the curves in Figure 9 (b). In the southern region, the results are

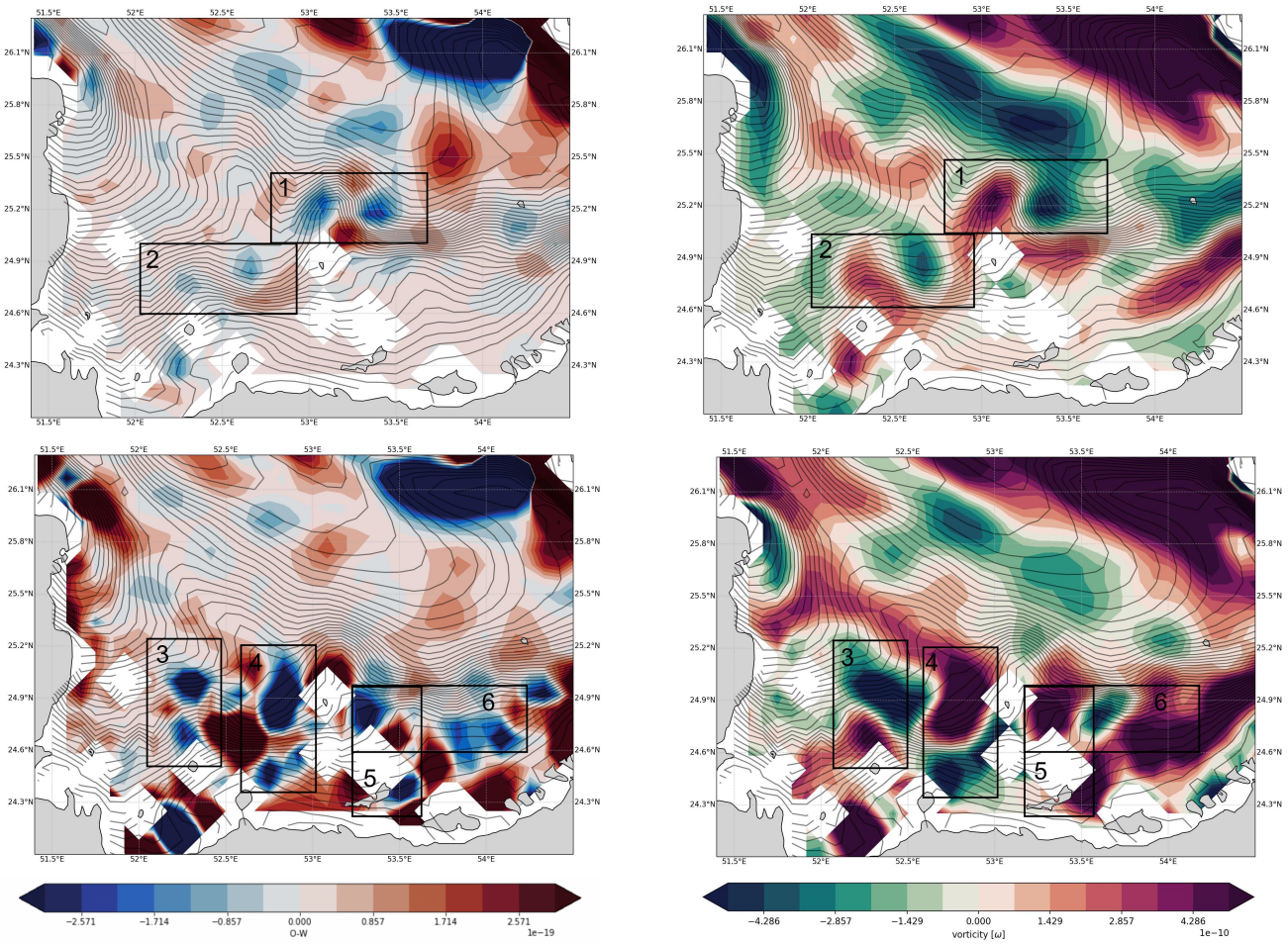

Figure 8: Okubo-weiss parameters with isohaline represented by black line computed from CMEMS left panel: first periode study (21-25 may 2014); right panel: second periode study (26-30 may 2014). Black boxes represente dipole of meso-vortex identified

more complex to interpret, as this area is very shallow and is the site of strong evaporation. It is in this part of the basin that the saltier waters are formed, which are then mixed with the other water masses of the basin, resulting in the Persian Gulf Water. Although the dispersion of this water in the Indian Ocean is well studied and documented (L'Hégaret et al., 2021), the phenomenon of formation of this very salty water is hardly known.

3.3.2 Vertical structure

The localisation of the section we study in is given Figure 5. The section A, is located at the east and mid latitude of the zone we are intererested in. It crosses a area were the frontogenesis is high as shown on Figure 5. The western part of the section starts at the center of the dipole; the distribution of salinity is not uniform along the section. The easternmost part seems to be more homogeneous and salty than the western part. This part is clearly more stratified on the vertical. Furthermore, the isohaline contours are denser in the centre of the section, between 30km and 40km, comfirming the intensification of the salinity gradient. The relative vorticity axis shows that the section crosses a cyclonic structure. Two upwellings of salty water occurs at 19 km and 47 km which coincide with

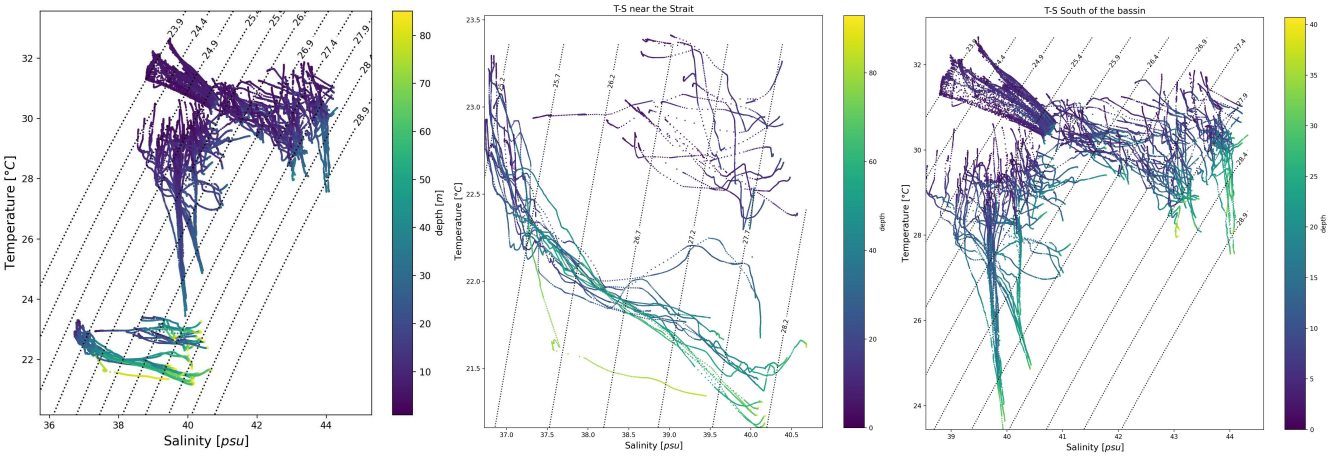

Figure 9: a) T-S diagram for all the mesurment of PHYSINDIEN 2014 inside the gulf ; b) T-S diagram for the mesurement near the strait,; c) T-S diagram for the mesurement south of the bassin

the edges of the vortex and show the presence of filaments at the periphery of the structure.

Section B is located to the south west of section A. At the surface the salinity gradient it crosses is weaker than the one crossed by section A. However, it is clearer that section B crosses a haline front as there are two completely different parts of the section, on the east side, the water is saltier and more homogeneous, while the west side is more stratified, with the isohaline curves tilted vertically at the surface and more steeply with depth. This indicates that the front separating the two waters is not vertical, which may be due to the tidal effect and to friction. Furthermore, the more stratified part is the one where the frontogenesis function is positive, indicating the dynamics of the front intensification, whereas in the eastern part the frontogenesis function is negative and coincides with the centre of an anticyclonic vortex. One result is that anticyclonic vortices relax the salinity gradient.

Sections C and D are longer and, are located in the southeastern part of the basin; this is why the observed salinity is much higher (Figure 11). The eastern part of section C crosses a front between 75 and 80 km: this place marks the transition between two very different stratifications. The southwestern part of the section is much more homogeneous although we can note the presence of upwellings of salty water at 21, 47 and 65 km which coincide with the extremity of a zone with positive vorticity, which indicates the presence of filaments The northeastern part is relatively strongly stratified, and shows the presence of fronts. We notice that the isohalins are not quite vertical. This area has a strongly negative frontogenesis and again in the center of a positive vorticity structure. This indicates that the frond tends to be relaxed.

The D section has a particular salinity distribution. In fact a front is located between 10 and 20 km, which separates a cooler water from a more homogeneous water; a second zone at 50 and 60 km has a strong salinity gradient and separates a water even more salty. Given the length of the section, the time needed to make the measurements is 12 hours. We can therefore deduce that these two fronts are in fact only one which has been affected by the effects of the tide and thus an aliasing effect. However, the front at 20 km coincides with a negative frontogenesis zone. We can therefore deduce a relaxation of the front.

The zone of homogeneous water coincid as well with the result exected regarding the Simpson-Hunter Criterion (Pitek, 2022). The topography of the bassin stronghly impacts the front generation and its dynamics.

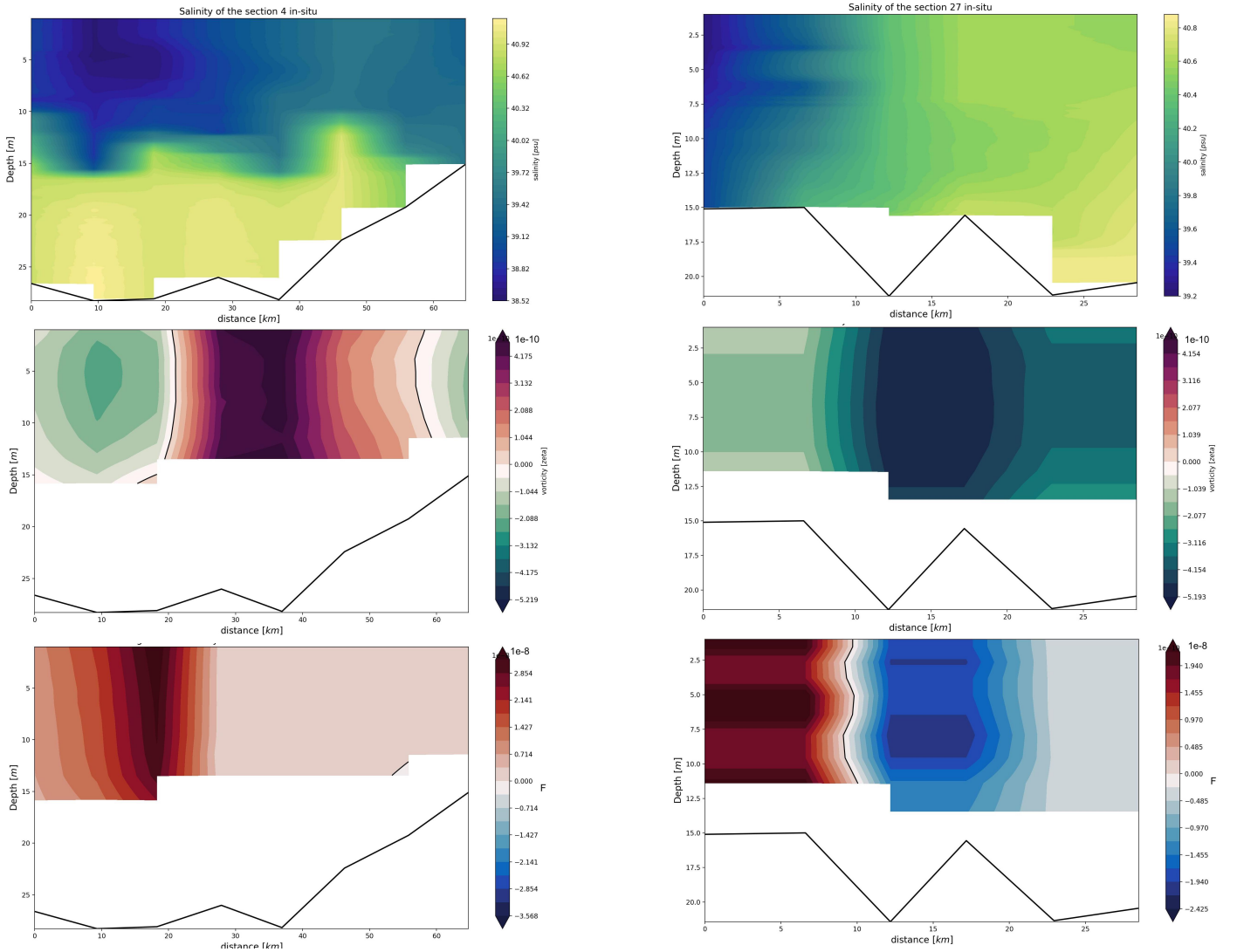

Figure 10: At the left the Section A, at the right the section B. Both had been measured during the first periode of the campagne. Top panel represent the salinity on the 0xz plan. middle pannel show the relative vorticity following **k** on the 0xz plan. Lower pannel show Frontogeneseis following **k** on the 0xz plan.The location of the section are given Figure 5

3.4 *Dynamics of the front relative to the structures*

The tide advects the front as shown by periodicity on the salinity signal. That means that the dynamics of the front will be a tidal oscillation and the alternance of the relaxation and straightening of the salt front. This effect can not be clearly observed either with the satellite, nor with the in situ observations because of the temporal resolution and the aliasing effect. The wind will have a more erratic effect on the salt front as its periodicity is not clear and therefore it will tend to displace and deform the front by its immediate action but will also feed mesoscale and submesoscale structures. These structures have a more complex effect on the dynamics of the front. A conter rotative dipole will tend to strenghen the front but also to bend it in the 0xy plane following the streamfunction. At the opposite, a rotational orientation like dipole tends to weaken the front.

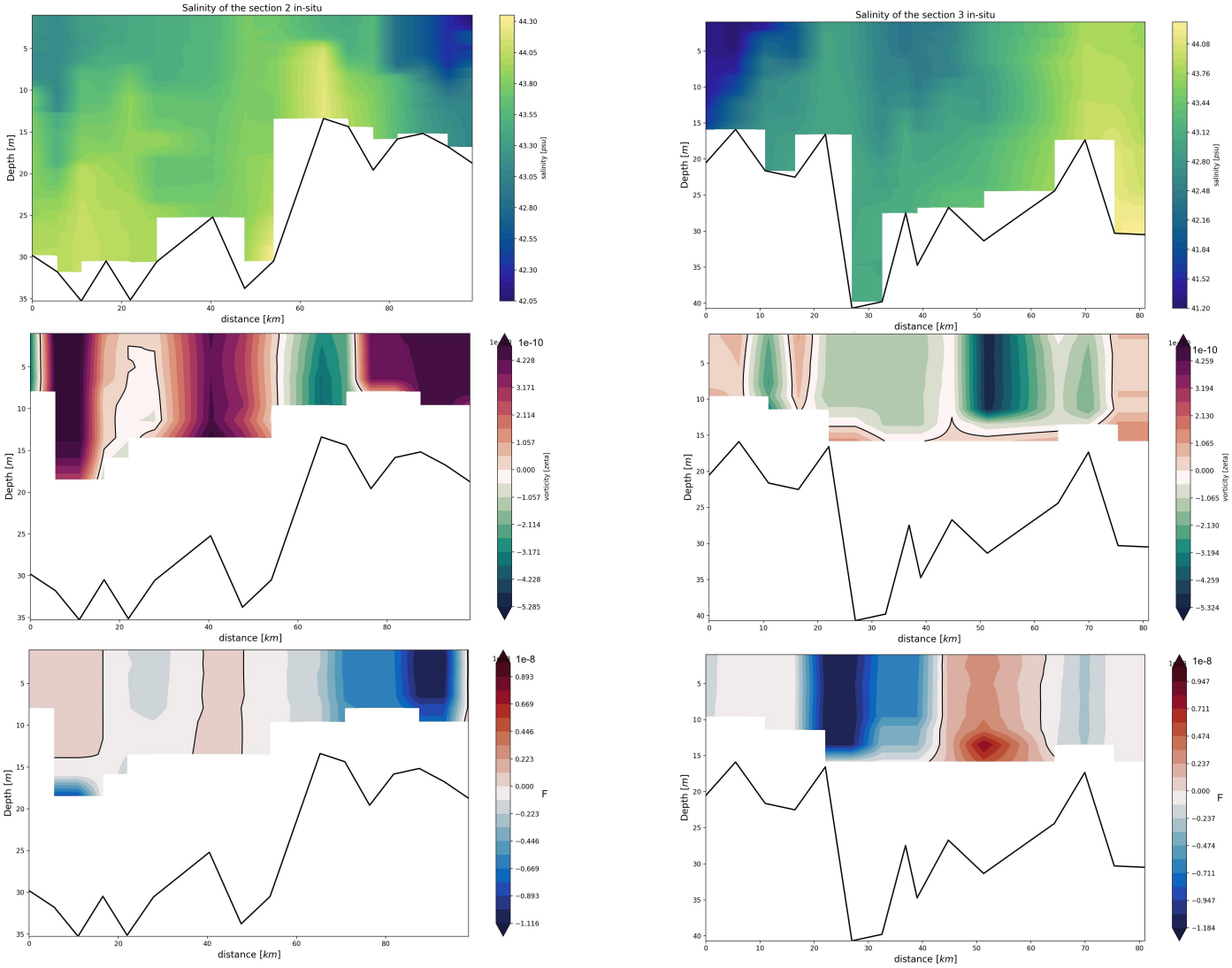

Figure 11: At the left the Section C, at the right the section D. Both had been measured during the second periode of the campagne. Top panel represent the salinity on the 0xz plan. middle pannel show the relative vorticity following **k** on the 0xz plan. Lower pannel show Frontogenesis on the 0xz plan.

4 Discussion and perspective

The use of in situ measurements, satellite data, and models have shown that the salinity fronts are concentrated in the southern Gulf. Reynolds (1993) had shown the presence of a strong gradient in this region but only with data measured in winter (see fig 9, Reynolds, 1993). In this area, two frontogenesis hot spots have been identified, which are strongly impacted by surface structures. Indeed, we could observe the reinforcing and advective impact of a counter rotating dipole on the isohaline. Their advection has also been observed on the thermal front near Ushant but only in the case of an isolated vortex (R.D. Pingree 1978; A. Le Boyet et al., 2009). A cyclonic vortex pair relaxes the front. Moreover, it has been observed that salt water upwelling occurs at the edges of the vortex.

The results obtained from the frontogenesis calculation must be interpreted with caution.The SST data are not high resolution data (1km). Furthermore the assumption that salinity is conserved in a

Lagrangian manner is based on the appendix sacling. But an uncertainty remains on the value of the vertical diffusivity which was considered as $K_v = 10^{-3}m^2.s{-}1$ for lack of data in the Persian Gulf. This confirms the need for specific measurements by VMP (Vertical Microstructure Profilers).

The time range used represents the duration of measurements made by the PHYSINDIEN campaign in 2014 in the southwestern basin and extends from 21 to 30 May 2014. This duration being of the order of a week, the altimeter data, especially AVISO data must be interpreted with caution because only a small part of the Gulf is scanned by the satellite. The rest of the data is obtained with a spatial and temporal interpolation. Thus the diagnosis of velocity components made on Gecko data depends on the consistency of altimeter data.

This could also explain the divergence of the HYCOM model data reanalyzed with the altimetric data observed in this region of the basin. Indeed, the initial plan was to base our dynamic study on data from the HYCOM reanalysis model. However, these data were not at all consistent. Like the CMEMS product, the HYCOM model is known to be too dispersive, underestimating the salinity maximum by up to 3 psu. This shows the complexity of accurately modeling this region and thus motivate the need for more observations.

New perspectives on these measurements are envisaged with the launch of new observation programs such as SWOT (surface water and ocean topography) which will allow a significant increase in spatial accuracy for the altimeter survey. However tides gauges mooring network and currentmeter adapted to a very shallow basin remains essential for a better understanding of the physical phenomena of the Persian Gulf

Note:
The colors bar are not the same between the different graphs because of the high variability of the different values, namely the salinity through the different regions of the Gulf. Thus a color bar for each graph allow to better highlight the different gradient.

5 Acknowledgments

This study, which follows the work of L. Pitek (2022) has thus studied the dynamics of front in the southern part of the Gulf. The results and the code developed during the internship have been shared so that the work can be further pursued by researchers.

Appendix A: Assumption of a conserved salinity

$$\frac{dS}{dt} = \frac{E-P}{\rho_0}\frac{S_0}{h} + K_h\nabla_h^2 S + K_v\partial_{zz}^2 S$$

WIth $E-P$ the evaporation/precipitation difference, K_h, K_v the horizontale and vertical diffusivity
K_h can be neglecte because the horizontal diffusivity is very small
Taking $E-P = 2m/year$, a reasonable value for the Persian Gulf
$h = 35m$ the mean depth in the Gulf
$S_0 = 35psu$ the main salinity
$K_v = 10^{-3}m^2.s{-}1$ We can scale

$$\frac{dS}{dt} = \frac{2}{365.86400} + 10^{-3}\frac{35}{35^2} = 6,34.10^{-8} + 2,8.10^{-5} \approx 2,8.10^{-5}psu/s$$

Then for 4 days the periode we use

$$\frac{\nabla S}{periode} = 0.4psu$$

Our hypothesis stand in regard to the variation of salinity near a front in the Persian Gulf, near 6 psu. As explained in the discussion, the value $K_v = 10^{-3}m^2.s{-}1$ is a rough guess of vertical diffusivity.

Appendix B: Frontogenesis function

We consider a quantity c conserved from a Lagrangian view, ie

$$\frac{dc}{dt} = \partial_t c + (\mathbf{u}.\nabla)\mathbf{c} = \mathbf{S}(\mathbf{c}) = \mathbf{0}$$

With S the source or sink of c
Taking the divergence,

$$\partial_t(\nabla\mathbf{c}) + \mathbf{u}.\nabla(\nabla\mathbf{c}) + \nabla\mathbf{u}.\nabla\mathbf{c} = \mathbf{0}$$

multiplying by the gradient of T,

$$\nabla c.\partial_t(\nabla\mathbf{c}) + \nabla\mathbf{c}\nabla\mathbf{u}.\nabla\mathbf{c} = \mathbf{0}$$

Then

$$\frac{1}{2}\partial_t \ \|\nabla\mathbf{c}\|^{\mathbf{2}} = -\nabla\mathbf{c}\nabla\mathbf{u}.\nabla\mathbf{c}$$

The frontogenesis function for a conserved quantity from a Lagrangian view is thus :

$$F(c,u) = -\nabla c\nabla\mathbf{u}.\nabla\mathbf{c}$$

It gives in 2D :

$$\frac{1}{2}\partial_t\|\nabla\mathbf{c}\|^{\mathbf{2}} = -(\partial_{\mathbf{x}}\mathbf{c})^{\mathbf{2}}\partial_{\mathbf{x}}\mathbf{u} - (\partial_{\mathbf{x}}\mathbf{v} + \partial_{\mathbf{y}}\mathbf{u})\partial_{\mathbf{x}}\mathbf{c}.\partial_{\mathbf{y}}\mathbf{c} - (\partial_{\mathbf{y}}\mathbf{c})^{\mathbf{2}}\partial_{\mathbf{y}}\mathbf{v}$$

with u (resp. v) the velocity in the the x (resp. y) direction

Reference

Cassianides, A., Martinez, E., Maes, C., Xavier, C., Gorgues, T., 2020. Monitoring the Influence of the Mesoscale Ocean Dynamics on Phytoplanktonic Plumes around the Marquesas Islands Using Multi-Satellite Missions. Remote Sensing 12. https://doi.org/10.3390/rs12162520

Defant A., 1961. Physical oceanography. New York: Pergamon Press.

Hoskins, B.J., 1982. The Mathematical Theory of Frontogenesis. Annu. Rev. Fluid Mech. 14, 131–151. https://doi.org/10.1146/annurev.fl.14.010182.001023

Le Boyer, A., Cambon, G., Daniault, N., Herbette, S., Le Cann, B., Marie, L., Morin, P., 2009. Observations of the Ushant tidal front in September 2007. Cont. Shelf Res. 29, 1026–1037. https://doi.org/10.1016/j.csr.2008.12.020

L'Hegaret, P., de Marez, C., Morvan, M., Meunier, T., Carton, X., 2021. Spreading and Vertical

Structure of the Persian Gulf and Red Sea Outflows in the Northwestern Indian Ocean. J. Geophys. Res.-Oceans 126, e2019JC015983. https://doi.org/10.1029/2019JC015983

McWilliams, J.C., 2021. Oceanic Frontogenesis, in: Carlson, C.A., Giovannoni, S.J. (Eds.), Annual Review of Marine Science, Vol 13, 2021. Annual Reviews, Palo Alto, pp. 227–253. https://doi.org/10.1146/annurev-marine-032320-120725

Merle, J., "Océan et climat," IRD Éditions, 2006

Michael Reynolds, R., 1993. Physical oceanography of the Gulf, Strait of Hormuz, and the Gulf of Oman—Results from the Mt Mitchell expedition. Marine Pollution Bulletin 27, 35–59. https://doi.org/10.1016/0025-326X(93)90007-7

Morvan, M., n.d. Impacts des tourbillons de méso et sous-mésoéchelle dans les golfes d'Oman et d'Aden sur les outflows du Golfe Persique et la Mer Rouge 171.

Okubo, A., 1970. Horizontal dispersion of floatable particles in the vicinity of velocity singularities such as convergences. Deep Sea Research and Oceanographic Abstracts 17, 445–454. https://doi.org/10.1016/0011-7471(70)90059-8

Open University course team, "Ocean Circulation," Pergamon Press

Pingree, R.D., 1978. Cyclonic eddies and cross-frontal mixing. Journal of the Marine Biological Association of the United Kingdom 58 (4), 955–963.“

Pitek, L "Evolution de la salinité, de la temperature et des fronts thermohalins dans le Golfe Persique, de Fevrier à Mai 2014", Report of internship at IUEM

Pous, S., 2005. Dynamique océanique dans les golfes Persique et d'Oman (phdthesis). Université de Bretagne Occidentale.

Pous, S., Lazure, P., Carton, X., 2012. A Process Study of the Tidal Circulation in the Persian Gulf. Open J. Mar. Sciences, 2, 4, 131-140. https://doi.org/10.4236/ojms.2012.24016

Pous, S., Lazure, P., Carton, X., 2013. A Process Study of the Wind-Induced Circulation in the Persian Gulf. Open J. Mar. Sciences, 3, 1, 1-11

Pous, S., Lazure, P., Carton, X., 2015. A model of the general circulation in the Persian Gulf and in the Strait of Hormuz: Intraseasonal to interannual variability. Cont. Shelf Res. 94, 55–70. https://doi.org/10.1016/j.csr.2014.12.008

Rahnemania, A., Bidokhti, A.A., Ezam, M., Lari, K., Ghader, S., 2019. A Numerical Study of the Frontal System between the Inflow and Outflow Waters in the Persian Gulf. J. Appl. Fluid Mech. 12, 1475–1486. https://doi.org/10.29252/jafm.12.05.29770

Sudre, J., Maes, C., Garcon, V., 2013. On the global estimates of geostrophic and Ekman surface currents. Limnology and Oceanography: Fluids and Environments 3, 1–20.

https://doi.org/10.1215/21573689-2071927

Weiss, J., 1991. The dynamics of entropy transfer in two-dimensional hydrodynamics. https://doi.org/10.1016/0167-2789(91)90088-Q